Steady axisymmetric flow in an open cylindrical container with a partially rotating bottom wall

M. Piva[a)]
Grupo de Medios Porosos, Facultad de Ingeniería, Universidad de Buenos Aires, Paseo Colon 850, (1063) Buenos Aires, Argentina

E. Meiburg[b)]
Department of Mechanical and Environmental Engineering, University of California at Santa Barbara, Santa Barbara, California 93106

(Received 28 October 2004; accepted 4 April 2005; published online 2 June 2005)

The steady motion of a viscous fluid in a cylindrical container with a partially rotating bottom wall and a free surface is investigated by means of axisymmetric Navier–Stokes simulations. The flow above the spinning disk at the center of the bottom wall is dominated by an Ekman boundary layer that drives the fluid radially *outward*. In contrast, an *inward* flow ensues along the outer, stationary part of the bottom wall, where the radially increasing pressure distribution set up by the rotating fluid motion near the free surface is not balanced by a corresponding centrifugal force. As a result, flow separation occurs at an intermediate radial location close to the outer edge of the rotating disk. Thus a flow configuration results that is dominated by a meridional vortex above the spinning disk, and a counterrotating vortex above the stationary part of the bottom wall. Simulations are conducted for various aspect ratios and Reynolds numbers, in order to evaluate the resulting changes in the vortex breakdown configurations. As the ratio of container radius to disk radius increases above a value of about 2.3, the influence of the lateral container wall on the features of the central flow in the neighborhood of the spinning disk becomes insignificant. By means of a simplified model problem, it is demonstrated that this rapid loss of influence is due to the exponential decay of the azimuthal surface velocity beyond the edge of the disk. This exponential decay is confirmed by the numerical data, and it reflects the fact that as the lateral wall moves outward, the stationary part of the end wall becomes the main sink for the azimuthal momentum of the fluid. © *2005 American Institute of Physics*. [DOI: 10.1063/1.1932664]

I. INTRODUCTION

Swirling fluid motion generated in a cylindrical container with one or two rotating end walls is known to give rise to a variety of vortex breakdown configurations, even under steady, laminar, and axisymmetric conditions. These features offer the opportunity for very "clean" observations of the conditions leading to vortex breakdown. Furthermore, the experimental setup is quite simple, and numerical simulations can be conducted with relative ease. Thus, it is no surprise that nominally axisymmetric swirling flows in cylindrical containers have become a popular model for developing and testing hypotheses regarding the origins of vortex breakdown, as well as its control.

The basic configuration consists of a closed cylindrical container with one rotating end wall. It gives rise to only two dimensionless parameters, viz., a Reynolds number $\mathrm{Re}=\Omega R_d^2/\nu$ based on the angular velocity Ω and the radius R_d of the spinning disk that forms the end wall of the container, and a geometric aspect ratio $\Gamma=H/R_d$, where H denotes the container height. In accordance with von Karman's analysis of the flow generated by a spinning disk in an unbounded fluid,[1] the rotating end wall attracts fluid from the central region of the container, and accelerates it radially outwards in an Ekman boundary layer of thickness $\mathrm{Re}^{-0.5}$. As it approaches the corner, the fluid turns and subsequently spirals along the cylindrical wall towards the opposite end of the container. The angular velocity of the fluid outside the wall boundary layer generates a centrifugal force, which has to be balanced by a radial pressure gradient. Next to the stationary end wall there exists a narrow boundary layer where the angular velocity is substantially reduced, so that it no longer balances the radial pressure gradient, which hence forces the fluid back towards the centerline. There it separates from the stationary end wall and flows back towards the rotating end wall, thus completing its meridional circulation.

A first series of flow visualization experiments for this setup was conducted by Vogel,[2,3] who reported a vortex breakdown region along the rotation axis, and away from the end walls. A systematic variation of the governing parameters by Escudier[4] revealed flow states with two or even three successive breakdowns, as well as a transition towards unsteady flows. These experimental observations led the author to hypothesize that the vortex breakdown phenomenon is inherently axisymmetric. Any departures from this axisymmetry are then due to an instability of the axisymmetric base state. For swirling jets, this point of view was recently confirmed by the three-dimensional simulations and compu-

[a)]Electronic mail: mpiva@fi.uba.ar
[b)]Author to whom correspondence should be addressed. Electronic mail: meiburg@engineering.ucsb.edu

tational linear stability analysis of Ruith *et al.*,[5] as well as by the investigation of swirling flows in pipes by Herrada *et al.*[6]

Following initial numerical simulations of the swirling flow in a closed container by Lugt and Haussling[7] as well as Lugt and Abboud,[8] Lopez,[9] and Brown and Lopez[10] provided a detailed analysis of the underlying physical mechanisms, based on numerical simulations. They demonstrate the existence of a standing centrifugal wave, whose amplitude increases with the Reynolds number. Eventually it becomes sufficiently large to create a stagnation point on the cylinder axis, which signals the inception of vortex breakdown. Emphasizing the importance of creating negative azimuthal vorticity, Brown and Lopez proceed to formulate a criterion for the prediction of vortex breakdown in terms of the helix angles of the velocity and vorticity vectors. More recently, Herrada and Shtern[11] have employed the same geometry to investigate vortex breakdown control by means of adding near-axis swirl, as well as externally imposed temperature gradients. Frequently this geometry, or slight variations thereof, have been employed as laboratory models for atmospheric vortices.[12–14]

By replacing the stationary end wall with a free surface, Spohn *et al.*[15,16] consider a geometrically similar configuration, which nevertheless gives rise to quite different physical mechanisms. Due to the absence of tangential stresses, a boundary layer does not form at the free surface, so that the inward spiraling fluid elements maintain their angular momentum. When the related centrifugal force is sufficiently large to balance the radial pressure gradient, the flow separates from the free surface, thereby forming a vortex breakdown bubble that is attached to the free surface. While a small amount of free surface deformation cannot be avoided in these experiments, corresponding numerical simulations for a flat, stress-free surface by Daube[17] confirm these findings for the axisymmetric case.

In a series of subsequent papers, several authors investigate the linear stability of the axisymmetric base state and the role of surface deflections within these instability modes. Valentine and Jahnke,[18] Lopez,[19] and Brons *et al.*[20] identify axisymmetric instability modes both with and without surface deflections, which set in via Hopf bifurcations. However, these modes develop at relatively high Reynolds numbers. Lopez *et al.*[21] and Lopez and Marques[22] observe azimuthal modes that become unstable at lower Reynolds numbers varying between about 1500 for shallow systems ($\Gamma<1$) and 1900 for deep systems ($\Gamma>1$), cf. also Young *et al.*,[23] Hirsa *et al.*[24] and Miraghaie *et al.*[25] For deep systems, the instability mode is concentrated in the near wall jet that forms as the bottom wall boundary layer is turned upwards by the lateral wall. This instability mode does not lead to a surface deflection, so that it can be captured in numerical simulations assuming a flat, stress-free surface. For shallow systems, on the other hand, the instability is focused in the region where the core fluid in a state of near-solid-body rotation encounters the outer fluid subject to strong meridional circulation. This mode results in a deflection of the free surface, so that it cannot be captured under the assumption of a flat surface.

The investigations of free surface flows beginning with the work of Spohn *et al.*[15,16] confirm the sensitivity of both the global flow field and the more localized vortex breakdown phenomenon to the nature of the boundary conditions. In this context, the role of the lateral wall location is not yet well understood. Both in the closed and the open container flows, this lateral boundary is responsible for turning the fluid away from the rotating end wall. It furthermore imposes tangential stresses on the fluid that result in the formation of a boundary layer, which acts as a sink of angular momentum. Hence it will be interesting to investigate how the fluid flow is modified if the cylindrical wall is moved radially outward, while keeping the radius of the rotating disk unchanged. In other words, we consider an open cylindrical container with a rotating disk embedded in an otherwise stationary bottom wall of radius R_c, cf. Fig. 1. This adds a further dimensionless parameter to the problem in the form of the aspect ratio $D=R_c/R_d$. Obviously, in this geometry the Ekman boundary layer does not have to turn upward at the outer edge of the rotating disk, and the fluid is free to move along the stationary bottom wall towards larger radii. However, it will lose some of its angular momentum in this way, which in turn will strongly affect the subsequent evolution of the flow. In the limit when the rotating disk extends only over a small part of the bottom wall, some guidance is provided by the classical investigation of Bödewadt.[26] This author studied the situation of a fluid in solid-body rotation above a stationary wall. Far away from the wall, the solid-body rotation generates a radially increasing pressure field. In the viscous boundary layer next to the stationary wall, the fluid is decelerated, so that this pressure gradient wins over the centrifugal forces and drives the fluid inward towards the center. Thus in a container with partially rotating bottom wall, the interesting situation arises that the fluid is driven *outward* above the rotating section of the wall, whereas it should be driven *inward* above the nonrotating section, provided the container is sufficiently large. Consequently, the boundary layer can be expected to separate from the bottom wall at some intermediate radius. However, whether this separation will occur on the rotating or the stationary segment of the bottom wall, and

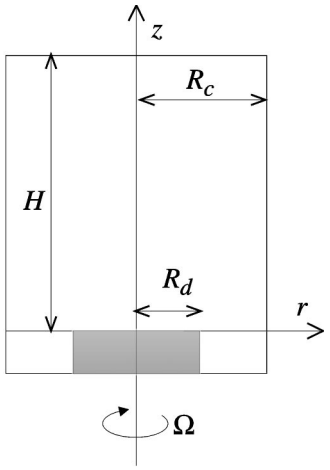

FIG. 1. Schematic of the physical problem. Within a cylindrical container of radius R_c, fluid motion is generated by a rotating disk of radius R_d, which forms part of the bottom wall. The fluid has a free surface at $z=H$.

where the flow might reattach again, is difficult to predict. These are some of the issues to be addressed in the following, by means of numerical simulations of the axisymmetric Navier–Stokes equations. In light of the above observations by other authors of three-dimensional instability modes setting in above Reynolds numbers of 1500–2000, we will limit the value of Re to 2000 in our investigation of axisymmetric base flows. The stability properties of these base flows are to be studied in a subsequent investigation. To summarize, we expect the axisymmetric swirling flows in cylinders with partially rotating bottom walls to exhibit qualitatively different features from their counterparts in containers whose entire end wall is in rotation. This can significantly affect such global features of the overall flow as, for example, their mixing efficiency.

The computational problem is formulated in Sec. II, while details with regard to the numerical procedure are provided in Sec. III. Subsequently, Sec. IV presents the results of the simulations. In a first step, we restrict our attention to the case $\Gamma=1$ and $D\geqslant 1$, i.e., the fluid column has a height equal to the disk radius, while the cylinder radius is equal to or larger than that of the disk. Thus, we focus on the effects of moving the lateral wall outward. Subsequently, the investigation will be extended to aspect ratios $\Gamma\neq 1$. Finally, Sec. V addresses surface deflections of the axisymmetric base state, and Sec. VI summarizes the main findings and presents the conclusions from this investigation.

II. PROBLEM FORMULATION

We consider a cylindrical container of radius R_c and height H, with a circular disk of radius R_d imbedded in the bottom boundary, cf. Fig. 1. At time $t=0$ the disk begins to rotate at a constant angular velocity Ω, thereby setting the fluid into motion. The lateral boundary and the bottom wall at radii larger than R_d are stationary, solid no-slip walls, while the top is formed by a horizontal, stress-free surface. The fluid is incompressible, with constant density and kinematic viscosity ν. The flow is described by the axisymmetric Navier–Stokes equations, formulated in cylindrical coordinates (r,ϕ,z), with the respective velocity components (u,v,w). Following Ref. 9, we avoid the explicit appearance of the pressure variable and identically satisfy the conservation of mass, by employing a streamfunction-vorticity formulation. Here, the streamfunction ψ is related to the radial and axial velocity components as

$$u=-\frac{1}{r}\frac{\partial\psi}{\partial z},\quad w=\frac{1}{r}\frac{\partial\psi}{\partial r}, \tag{1}$$

and to the azimuthal vorticity component as

$$\eta=-\frac{1}{r}\frac{\partial^2\psi}{\partial z^2}-\frac{\partial}{\partial r}\left(\frac{1}{r}\frac{\partial\psi}{\partial r}\right). \tag{2}$$

By scaling time with Ω^{-1}, length with R_d, and velocity with ΩR_d, the dimensionless Navier–Stokes equations take the form

$$\frac{\partial v}{\partial t}=\frac{1}{r}J(v)+\frac{1}{r}\frac{v}{r}\frac{\partial\psi}{\partial z}+\frac{1}{\mathrm{Re}}\left[\frac{\partial^2 v}{\partial z^2}+\frac{\partial^2 v}{\partial r^2}+\frac{1}{r}\frac{\partial v}{\partial r}-\frac{v}{r^2}\right], \tag{3}$$

$$\frac{\partial\eta}{\partial t}=J\left(\frac{\eta}{r}\right)+2\frac{v}{r}\frac{\partial v}{\partial z}+\frac{1}{\mathrm{Re}}\left[\frac{\partial^2\eta}{\partial z^2}+\frac{\partial^2\eta}{\partial r^2}+\frac{1}{r}\frac{\partial\eta}{\partial r}-\frac{\eta}{r^2}\right], \tag{4}$$

$$\frac{\partial^2\psi}{\partial z^2}+\frac{\partial^2\psi}{\partial r^2}-\frac{1}{r}\frac{\partial\psi}{\partial r}=-r\eta. \tag{5}$$

Here

$$J=\frac{\partial\psi}{\partial z}\frac{\partial}{\partial r}-\frac{\partial\psi}{\partial r}\frac{\partial}{\partial z} \tag{6}$$

and

$$\mathrm{Re}=\frac{\Omega R_d^2}{\nu}. \tag{7}$$

The boundary conditions take the form

$$0<z<\Gamma,\quad r=0:\ \psi=0,\quad v=0,\quad \eta=0, \tag{8}$$

$$0<z<\Gamma,\quad r=D:\ \psi=0,\quad v=0,\quad \eta=-\frac{1}{r}\frac{\partial^2\psi}{\partial r^2}, \tag{9}$$

$$z=0,\quad r\leqslant 1:\ \psi=0,\quad v=r,\quad \eta=-\frac{1}{r}\frac{\partial^2\psi}{\partial z^2}, \tag{10}$$

$$z=0,\quad r\geqslant 1:\ \psi=0,\quad v=0,\quad \eta=-\frac{1}{r}\frac{\partial^2\psi}{\partial z^2}, \tag{11}$$

$$z=\Gamma:\ \psi=0,\quad \frac{\partial v}{\partial z}=0,\quad \eta=0, \tag{12}$$

where the dimensionless parameters

$$\Gamma=\frac{H}{R_d},\quad D=\frac{R_c}{R_d} \tag{13}$$

are prescribed by the geometry of the problem. Note that we assume a flat, stress-free upper surface, which has worked well in the past in the context of characterizing axisymmetric base flows, e.g., see Ref. 17. When identifying potential instability modes to such base flows, on the other hand, this assumption may not be valid. The boundary conditions for the azimuthal vorticity η along the solid boundaries are obtained from the no-slip condition, which takes the form $\partial\psi/\partial r=0$ along $r=D$ and $\partial\psi/\partial z=0$ at $z=0$.

III. COMPUTATIONAL APPROACH

We employ a finite difference approach to simulate the system of equations (3)–(5) subject to the boundary conditions (8)–(12). The computational grid is equidistant, and the time-dependent solution is calculated until an essentially steady state is reached. At $t=0$, the fluid is at rest everywhere. For every time step, Eqs. (3) and (4) are advanced in time in order to update the azimuthal velocity and vorticity, respectively, by means of a standard second-order alternating

direction implicit (ADI) method, e.g., see Ref. 27. During this process, first-order accurate finite difference expressions of the second derivative of the streamfunction are employed as vorticity boundary conditions. Subsequently, the streamfunction at the new time level is evaluated from (5) by means of a standard full multigrid algorithm, in which line relaxation is used as the smoothing operator, e.g., see Ref. 28.

In order to smooth the discontinuity in the boundary conditions at the outer edge of the embedded disk, we employ a transition layer of thickness R_{tr} for the azimuthal wall velocity

$$v(z=0)=\frac{r}{2}\left(1-\tanh\left[\frac{(r-1)}{R_{tr}}\right]\right). \tag{14}$$

This provides an effective boundary condition of the form $v\sim r$ for $r\lesssim 1-R_{tr}$ and $v\sim 0$ for $r\gtrsim 1+R_{tr}$. In order to evaluate the sensitivity of the computed flow field to the value of R_{tr}, we conducted test simulations for $R_{tr}=n\Delta r$, with $n=2,4,6$ and Δr the grid spacing in the radial direction. For values of Re, Γ, and D within the range of interest, no dependence on n was observed, so that $n=2$ was employed for the simulations to be discussed below.

The appropriate spatial resolution was determined by simulating the case $D=1$, $\Gamma=1$, and $\mathrm{Re}=900$ for the three different grids of 65×65, 129×129 and 257×257 points. No significant differences in the computed flow patterns were observed between the medium and fine grids. Therefore, most simulations were conducted on a 129×129 grid. The code was further validated by comparing computed streamlines with experimental visualizations of steady dye lines obtained by one of the authors.[29] An example of such a comparison is shown in Fig. 2, where it can be seen that the computed streamlines for $\mathrm{Re}=1120$, $D=1$, and $\Gamma=1$ reproduce the features of the experimentally observed flow field with good accuracy. Finally, the code was also verified by comparing computed results for $D=1$ and different values of the Reynolds number with the experimental data obtained in Ref. 15. As will be discussed below, good agreement is observed.

The temporal evolution of the streamfunction at three sampling points $(1/3, \Gamma/2)$, $(1/2, \Gamma/2)$, and $(1/4, \Gamma/2)$ is monitored in order to check the overall convergence of the simulation to a steady state. The calculation was terminated when $\mathrm{abs}(\psi_{n+1}-\psi_n)<10^{-6}$ at all three points.

IV. RESULTS

A. $D=1$

As a first step, we present in Fig. 3 the flow for $\Gamma=1$, $\mathrm{Re}=900$, and the horizontal aspect ratio $D=1$. In this case, the entire bottom wall of the container rotates. The steady streamlines, along with the contours of the radial and axial velocity components and of the angular momentum $l=v\cdot r$, confirm the familiar picture.[15,17] Specifically, they demonstrate that the no-slip boundary condition at the rotating disk increases the angular fluid velocity in a narrow Ekman boundary layer, which results in the outward radial acceleration of the fluid just above the bottom wall. As this fluid reaches the neighborhood of the vertical container wall, it is deflected upward. Along the free surface, the flow is driven towards the center and then turned downward, thus completing its closed trajectory.

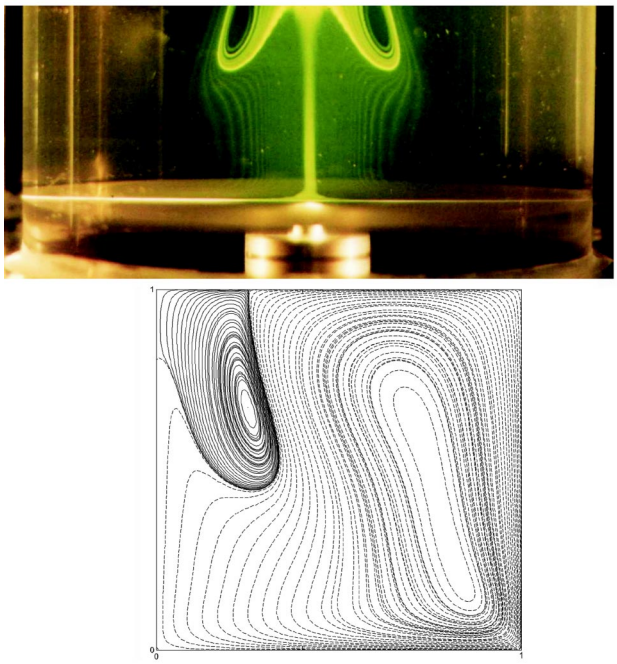

FIG. 2. (Color online). Flow field in a cylindrical container with a rotating bottom and a free surface: Comparison between experimental results and simulation for $\mathrm{Re}=1120$, $\Gamma=1$, and $D=1$. Top: snapshot of the meridional flow field obtained by dye injection (Ref. 29). Bottom: simulated streamlines in the r, z plane.

Across the entire container height, a pronounced vortex core develops for $r\lesssim 0.3$ in which the contour lines of angular momentum are nearly vertical, cf. Fig. 3(d). Here the azimuthal velocity increases approximately linearly with the radius, so that a nearly solid-body-like rotation exists. In this region the axial and radial velocity components are much smaller, as compared to the azimuthal one. Near the vertical container walls, the angular momentum of the upward flowing fluid is reduced due to the no-slip boundary condition, so that the l contours are deflected toward the center as the flow approaches the top boundary. No loss of angular momentum occurs at the free surface, due to the absence of tangential stresses, so that the azimuthal velocity of a fluid element increases as it moves inward towards the container axis. The resulting radial pressure gradient forces the inward flow to "separate" from the surface. This, in turn, gives rise to a closed vortex breakdown bubble attached to the free surface that had also been observed in the earlier experimental work of Ref. 15, as well as in the numerical simulations of Ref. 17. This bubble extends over more than half of the container height, cf. Fig. 3(a). As explained in the figure caption, for illustrative purposes an equal number of unevenly spaced contour lines are plotted above and below $\psi=0$, in order to reveal the bubble structure. However, we emphasize that the recirculating fluid inside the bubble has vertical and radial velocity components much smaller than the rest of the flow, as $\psi_{\min}/\psi_{\max}=2\times 10^{-2}$.

Figure 4 shows corresponding streamline configurations

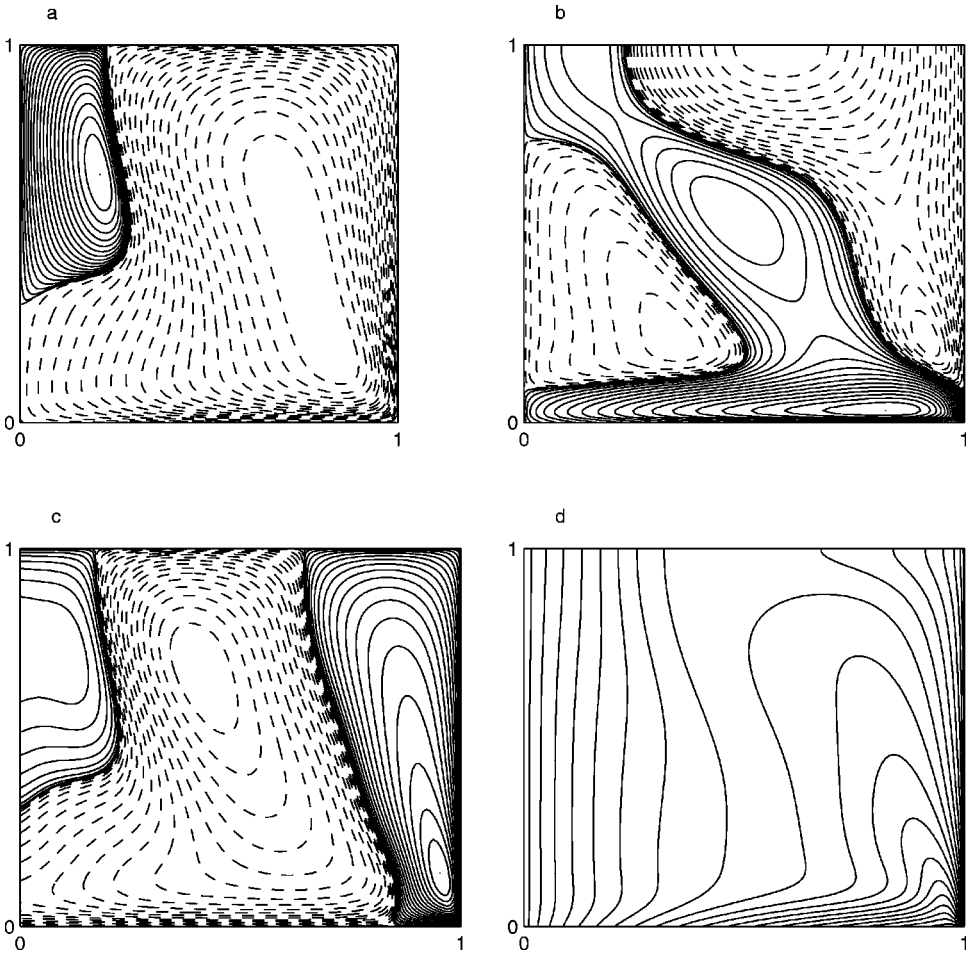

FIG. 3. Contours of (a) streamlines ($\psi_{\min}=-0.010$, $\psi_{\max}=2.1\times10^{-4}$); (b) radial velocity ($u_{\min}=-0.08$, $u_{\max}=0.15$); (c) axial velocity ($w_{\min}=-0.08$, $w_{\max}=0.12$); (d) angular momentum ($l_{\min}=0.0$, $l_{\max}=1.0$) in the meridional plane for Re=900, $\Gamma=1$, and $D=1$. For visualization purposes, the contour levels are nonuniformly spaced, with 20 positive and 20 negative values shown. The plotted contour levels are determined as level (i)=Max(variable)$\times(i/20)^3$ and level (i)=Min(variable)$\times(i/20)^3$, respectively. A vortex breakdown region is observed that is attached to the free surface.

for different values of Re. Below a value of $\mathrm{Re}_1\simeq405$, a breakdown region does not develop. For $\mathrm{Re}_1<\mathrm{Re}<\mathrm{Re}_2\simeq440$, a narrow bubble develops along a finite interval of the symmetry axis. This bubble is not attached to the top surface. With increasing Reynolds number this region grows in size, and its upper stagnation point approaches the surface. For $\mathrm{Re}>\mathrm{Re}_2$ the bubble grows in the radial direction along the free surface. Simultaneously, its lower stagnation point moves upward and eventually reaches the free surface for $\mathrm{Re}_3=940$. Thus, beyond Re_3 a closed recirculation torus exists that is attached to the free surface. The observed flow regimes and their dependence on the Reynolds number agree with the experimental data obtained in Ref. 15. This validates our computational approach, although it needs to be pointed out that the simulations yield slightly lower (by about 10%) values for Re_1 and Re_2, as compared to those reported for the experiments. This may be related to the fact that in the experiments the free surface was not perfectly flat. Spohn *et al.* report surface deflections up to about 10% of the container height.

B. Influence of the horizontal aspect ratio

For the reasons discussed in the introductory section, it will be interesting to observe the effects on the overall flow, and on the vortex breakdown configuration, of pushing the container walls radially outwards. For $D=3.33$, Fig. 5 depicts information corresponding to that provided in Fig. 3 for $D=1$. As before, the narrow boundary layer above the rotating disk embedded in the bottom wall is accelerated outwards in the radial direction. However, now it does not have to ascend abruptly at $r=1$. Instead, it continues to move in the radial direction beyond the edge of the spinning disk, all the way to a location r_{co} at which it separates from the bottom wall, cf. the close-up provided in Fig. 6. The reason behind this separation can be found in the description of the rotating fluid motion above a stationary wall by Bödewadt:[26] Far above the wall, the rotating fluid generates a radially increasing pressure field. In the viscous boundary layer next to the wall, the fluid is decelerated, so that this pressure gradient wins over the centrifugal forces and drives the fluid inward towards the center. Thus in a container with a partially rotating bottom wall, we observe the interesting situa-

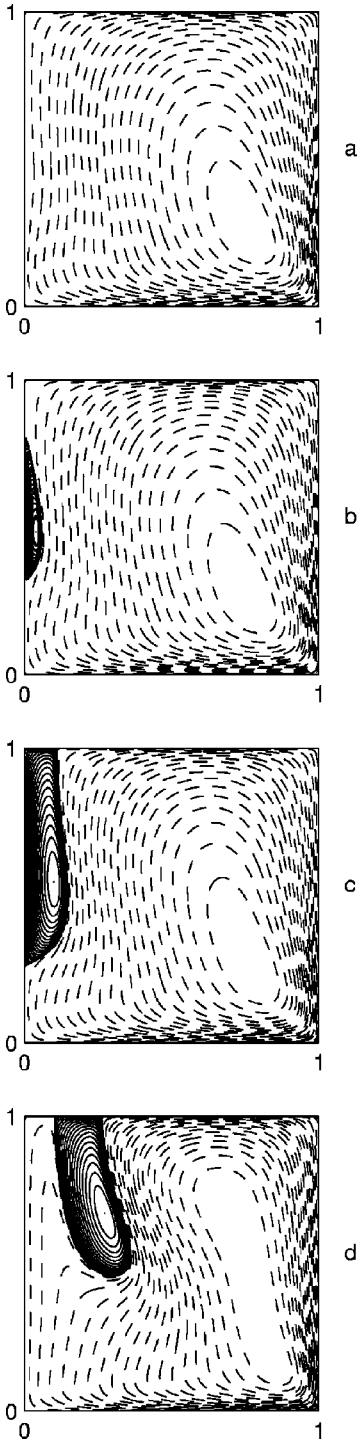

FIG. 4. Streamline patterns in the meridional plane for $\Gamma=1$, $D=1$, and (a) Re=400; (b) Re=425; (c) Re=500; (d) Re=1250. The internal bubble is first observed at $\mathrm{Re}_1=405$, and it becomes attached to the free surface at $\mathrm{Re}_2=440$. At $\mathrm{Re}_3=940$ the lower stagnation point of the recirculation region reaches the free surface, leading to the formation of a toroidal bubble structure. The above Re values are slightly below those reported in the experimental investigation in Ref. 15.

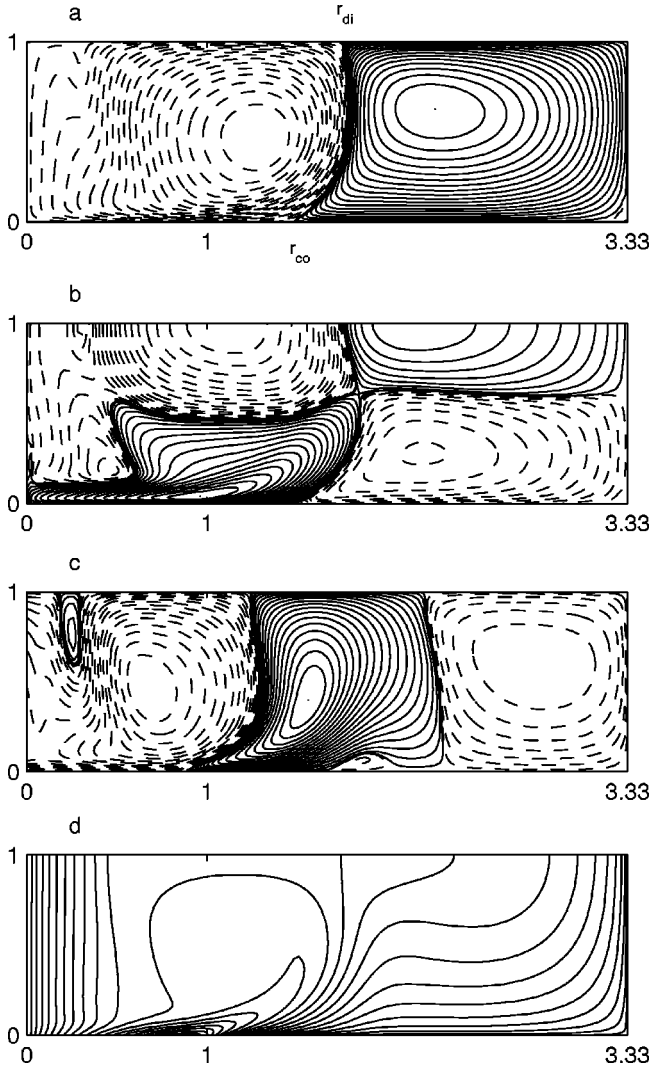

FIG. 5. Contours of (a) streamlines ($\psi_{\min}=-0.8\times10^{-3}$, $\psi_{\max}=2.6\times10^{-4}$); (b) radial velocity ($u_{\min}=-0.08$, $u_{\max}=0.16$); (c) axial velocity ($w_{\min}=-0.07$, $w_{\max}=0.06$); (d) angular momentum ($l_{\min}=0$, $l_{\max}=0.4$) in the meridional plane for Re=900, $\Gamma=1$, and $D=3.33$. The meridional flow is seen to separate from the stationary section of the bottom wall at radius r_{co}, and to reattach at the free surface at r_{di}. The streamline connecting r_{co} and r_{di} separates the outer, clockwise vortex, from the inner, counterclockwise one.

tion that the fluid is driven radially outward above the rotating disk, whereas it is driven inward above the section at rest. As a result, separation occurs at some intermediate location.

Upon separation, the fluid turns upward towards the free surface. The separation streamline, which connects with the free surface at r_{di}, demarcates the two main regions of the flow field, viz., an inner one with counterclockwise meridional circulation and an outer one characterized by circulation of the opposite sign. By comparing the streamline configurations in Figs. 3(a) and 5(a), it is obvious that the inner region is now substantially larger than for $D=1$. At the same

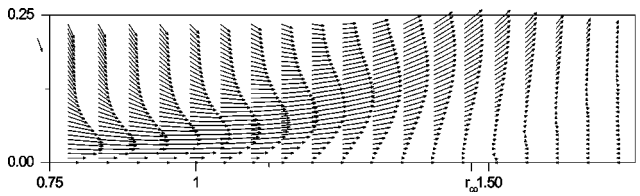

FIG. 6. Close-up of the flow near the separation location at r_{co}, for the flow conditions shown in Fig. 5 (Re=900, $\Gamma=1$, and $D=3.33$).

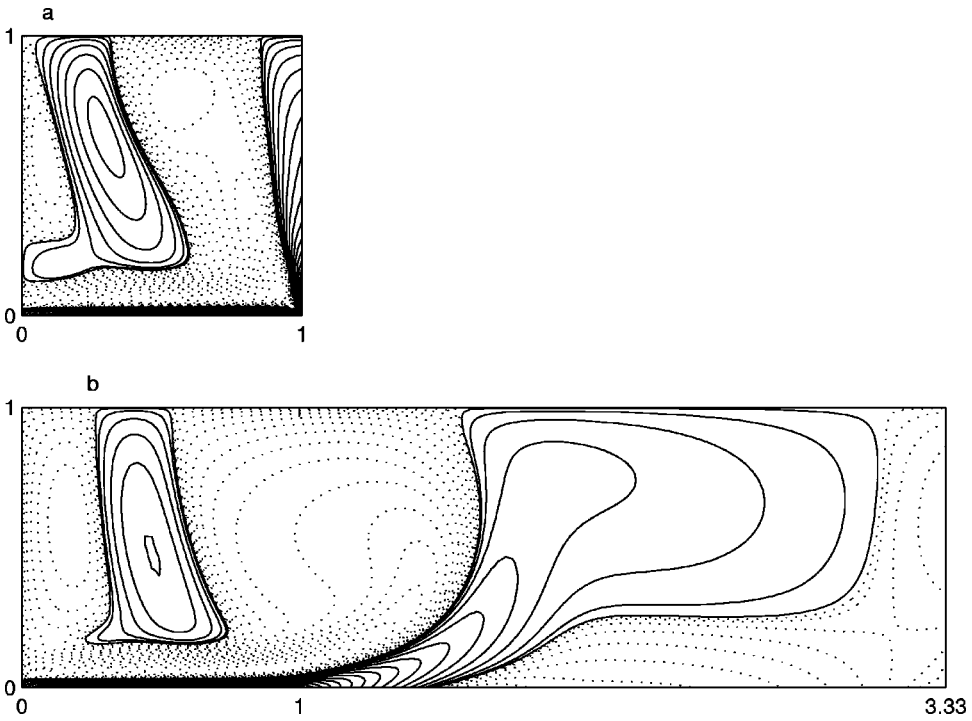

FIG. 7. Contour plots of the azimuthal vorticity component η for the flow conditions shown in Figs. 3 and 5. (a) Re=900, $\Gamma=1$, and $D=1$; (b) Re=900, $\Gamma=1$, and $D=3.33$. The separated layer of positive azimuthal vorticity results in the formation of the large-scale clockwise vortex at large radii.

time, the near-axis region of approximately solid-body-like rotation has grown, cf. Figs. 3(d) and 5(d). This reflects the diminished role of the vertical wall as a sink of angular momentum, due to its increased distance from the axis. Figure 5(a) indicates that the vortex breakdown bubble near the axis no longer forms, although there is a continued tendency of the return flow to separate from the free surface as it approaches the axis. This behavior will be discussed in more detail below.

To complete the comparison between the cases $D=1$ and $D=3.33$, we present in Fig. 7 contour plots of the azimuthal vorticity component η. For $D=1$, η is seen to be positive within the boundary layers adjacent to the rotating disk and the vertical wall, while it is negative along most of the free surface and in the interior, except for an annular region of positive η that is attached to the free surface and associated with the vortex breakdown phenomenon. For $D=3.33$ we observe a tongue of positive η separating from the stationary bottom wall. This separated layer extends all the way to the free surface, thereby setting up a large-scale clockwise vortex at large radii. The toroidal region of positive azimuthal vorticity attached to the free surface near the axis is not strong enough to result in a recirculation zone, although a tendency towards the formation of a vortex breakdown region is clearly visible in the streamline pattern of Fig. 5(a).

In the following, we will attempt to quantify the flow changes as functions of the aspect ratio D. Beyond a certain value of the aspect ratio, we expect the flow in the vicinity of the rotating disk no longer to depend on the exact location of the vertical container walls, since the loss of azimuthal momentum primarily occurs in the boundary layer along the stationary bottom wall, rather than in the boundary layer attached to the vertical wall. Hence one of the questions to be addressed below concerns the value of D beyond which this asymptotic state is reached, so that the flow field becomes largely independent of this parameter.

In this context, a simple model problem can provide some insight into how the flow field above the stationary bottom wall will decay in the radial direction beyond the edge of the spinning disk, for large values of the aspect ratio D: Consider a unidirectional, fully developed, steady flow $(u,0,0)$ in the Cartesian coordinate system (x,y,z), for the semi-infinite domain $y\geqslant 0$. At $z=0$ we have a solid wall where $u=0$, and at $z=1$ there is a free surface with $\partial u/\partial z=0$. By scaling the velocity with its value at $y=0$, $z=1$, we obtain $u(x,0,1)=1$. This situation represents a simple model of the actual flow field for radii $r>1$, where the curvature terms have been neglected. In the absence of any externally imposed pressure gradients, the u-velocity component is governed by the Laplace equation

$$\frac{\partial^2 u}{\partial y^2}+\frac{\partial^2 u}{\partial z^2}=0. \tag{15}$$

For the above set of boundary conditions, we obtain the solution

$$u(y,z)=e^{-(\pi/2)y}\sin\left(\frac{\pi}{2}z\right). \tag{16}$$

We observe that the characteristic length over which the u-velocity component decays in the y direction is $2/\pi$, and that this decay is exponential in nature.

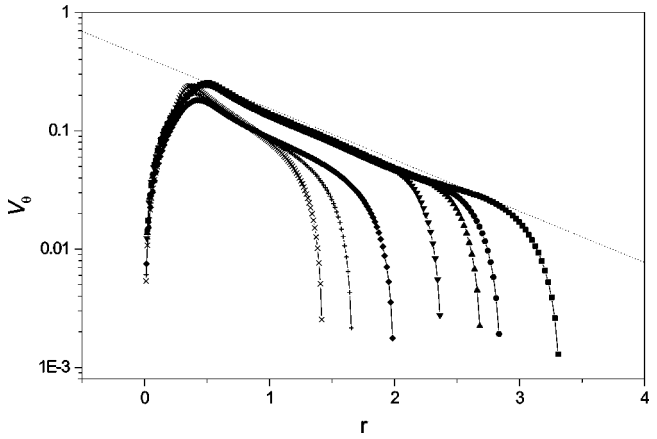

FIG. 8. Azimuthal velocity profiles at the free surface for $\Gamma=1$, Re=900, and various values of D; ×, $D=1.43$; +, $D=1.66$; ◆, $D=2$; ▼, $D=2.38$; ▲, $D=2.70$; ●, $D=2.86$; ■, $D=3.33$. The dotted line indicates proportionality to e^{-r}.

Figure 8 provides the corresponding information for the swirling flow problem under consideration, i.e., the decay of the azimuthal surface velocity component with r. We find that, in analogy to the above unidirectional model problem, this decay is exponential, albeit with a decay length of one, rather than $2/\pi$. This difference is due to the cylindrical nature of the problem, as opposed to the Cartesian model problem. Consequently, if the vertical wall is removed from the outer edge of the spinning disk by a distance substantially larger than unity, its influence on the azimuthal velocity profile near the edge of the disk should become negligible. Figure 8 confirms that for $D>2.3$ the location of the outer wall indeed becomes insignificant.

The exact location of the separation point depends on the relative strength of the outward boundary layer flow coming from the spinning disk, and the inward moving boundary layer above the stationary part of the bottom wall. The latter will be limited roughly to the region where a significant rotational velocity of the fluid at the free surface exists, i.e., to the region within one decay length of the outer edge of the spinning disk. We thus expect the separation location to be found within this region, which is confirmed by Fig. 5. The exact location will depend on the height of the container.

In order to investigate changes to the vortex breakdown region as a result of moving the vertical wall outward from the edge of the spinning disk, we discuss a series of simulations for which the Reynolds number and the vertical aspect ratio are fixed at Re=900 and $\Gamma=1$, respectively, while D is varied in the range of $1\leqslant D\leqslant 3.33$. A sequence of streamline plots for various values of D is depicted in Fig. 9. In all cases, the streamline corresponding to $\psi=0$ is plotted, in order to demonstrate the shapes of the separatrices. Figure 9(a) reproduces the flow structure discussed above for $D=1$, viz., a large-scale counterclockwise recirculation and a single bubble attached to the free surface. According to the nomenclature suggested by Brons *et al.*,[20] we will refer to this type of vortex breakdown region as corner bubble. The fluid inside this breakdown region rotates in the clockwise direction.

As D is slightly decreased to $D=1.43$, the lower stagnation point of the breakdown region on the axis moves upward. At the same time, a small clockwise corner vortex emerges in the lower right-hand corner of the cross section, as a result of the flow separation from the stationary part of the bottom wall. For $1.43<D<2$ the vortex breakdown region continues to shrink in size, while the corner vortex grows slightly, cf. Figs. 9(c) and 9(d).

In the range $2<D<2.38$, a large-scale reorganization of the flow takes place, cf. Fig. 9(e). First, the vortex breakdown region next to the axis disappears. In addition, after

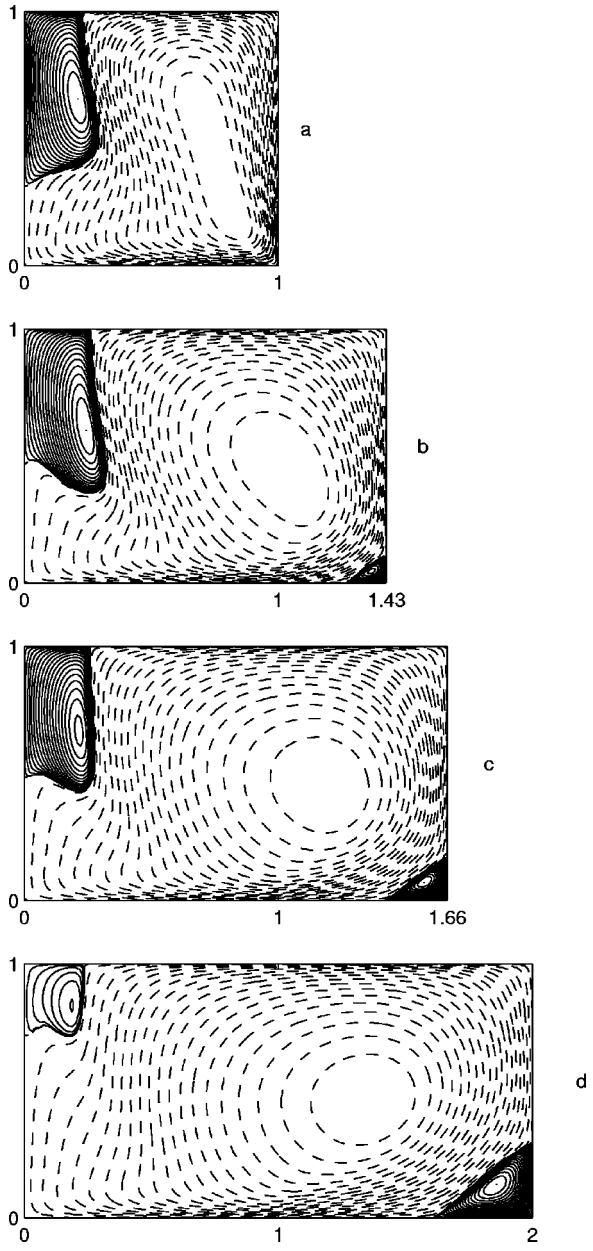

FIG. 9. Sequence of streamline plots in the meridional plane showing the effects of removing the cylinder wall from the outer edge of the rotating disk. Parameters are $\Gamma=1$, Re=900, and (a) $D=1$; (b) $D=1.43$; (c) $D=1.66$; (d) $D=2$; (e) $D=2.38$; (f) $D=2.70$; (g) $D=2.86$; (h) $D=3.33$. As D increases, a secondary vortex emerges in the lower right-hand corner of the cross section. This vortex grows with D, until for a critical value of D somewhat above 2 the reattachment point jumps from the vertical wall to the free surface. For $D>2.3$, the features of the inner vortex become independent of D.

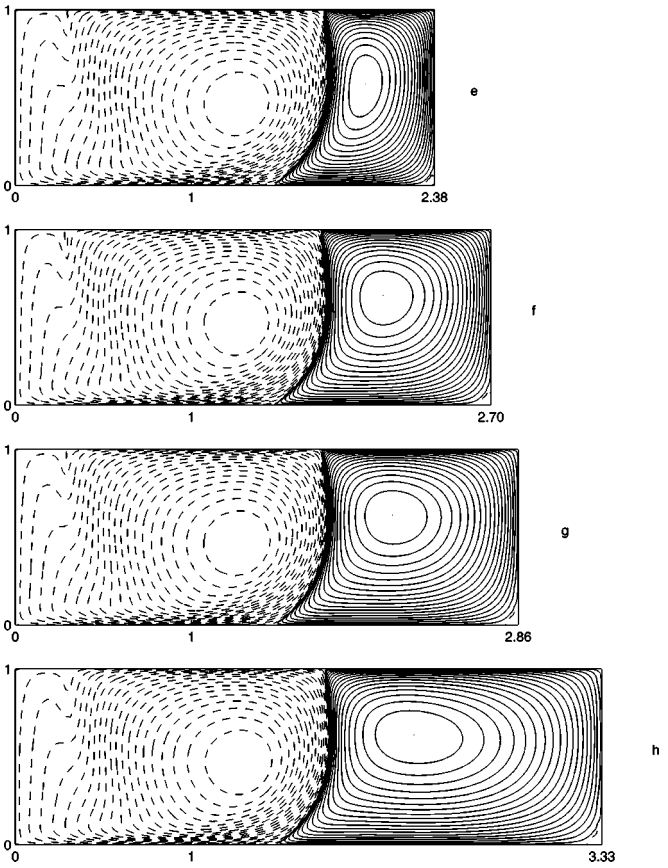

FIG. 9. (*Continued*).

separating from the stationary part of the container bottom, the flow no longer reattaches somewhere on the vertical wall. Instead, the tendency of the rotating free surface flow to form a clockwise vortex above the stationary bottom wall, as analyzed in Ref. 26, has grown sufficiently strong for the separatrix to reattach directly to the free surface. In this way, the corner vortex has transitioned to a large-scale recirculation region that occupies the outer region of the container over its entire height.

In the range $2.38 \leqslant D < 2.86$, the strongly curved streamlines at the surface near $r \approx 0.3$ indicate the tendency of the flow to form a weak toroidal vortex breakdown bubble away from the axis of rotation. Figure 10 shows that at the higher value of Re=1 300 such a recirculation bubble has indeed formed.

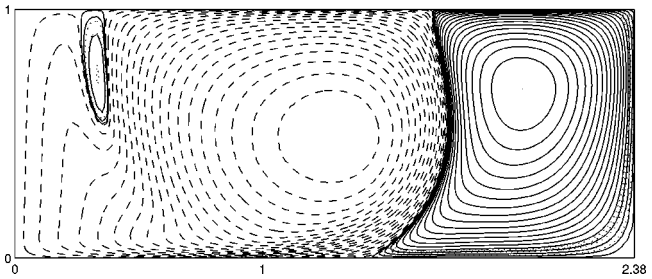

FIG. 10. Streamline contours for $\Gamma=1$, Re=1300, and $D=2.38$ show the existence of a toroidal recirculation region attached to the free surface, but away from the axis.

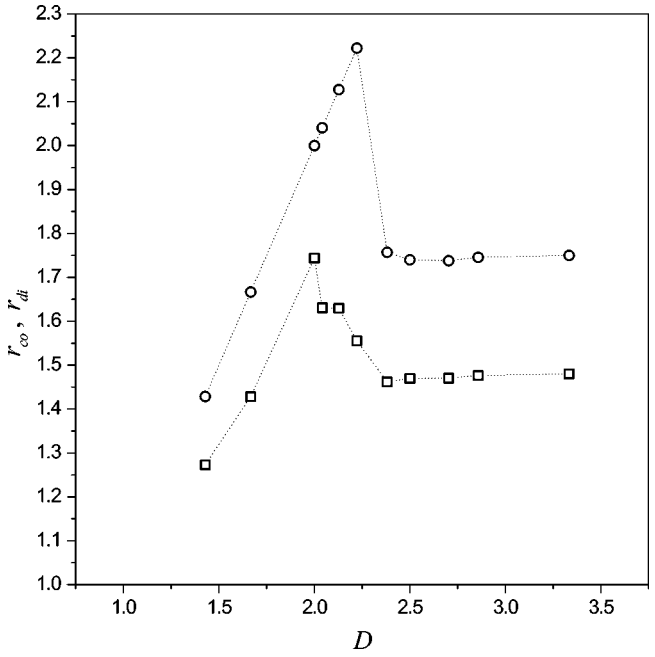

FIG. 11. The locations of separation (r_{co}, squares) and reattachment (r_{di}, circles), as functions of D. Above $D \approx 2.3$ these locations no longer vary with the aspect ratio.

The sequence of streamline plots in Fig. 9 confirms our above analysis regarding the decreasing influence of the vertical wall for large D, in that it shows the large-scale counterclockwise vortex above the rotating disk to remain unchanged once $D > 2.38$. This asymptotic behavior is furthermore confirmed by Fig. 11, which provides the separation (r_{co}) and reattachment (r_{di}) locations as functions of D.

Viewed from an energy point of view, the flow's independence of D above a critical value indicates that the energy injected into the flow by the rotating disk primarily serves to create and maintain the counterclockwise large-scale vortex above the spinning disk. In contrast, the outer-clockwise vortex contains relatively little kinetic energy, which resides mostly in the region just beyond the separatrix. Figure 12 presents data regarding the kinetic energy density k_i associated with the fluid in each of the large-scale vortices. Here $i=1$ (2) refers to the inner (outer) vortex, and k_i is defined as K_i/V_i, where K_i is the overall kinetic energy of vortex i, while V_i represents its volume.

k_1 is seen to decrease in the range $1 < D < 2$, indicating an overall slowdown of the primary vortex as the container walls are pushed outward. This can be explained by the momentum losses in the boundary layer along the stationary bottom wall. For $2 \lesssim D \lesssim 2.5$, the large-scale reorganization of the flow occurs, as mentioned above. The separating streamline no longer reattaches to the vertical container walls, and instead directly joins the free surface. This results in an abrupt reduction of the volume occupied by the inner vortex, so that its kinetic energy density increases. k_1 remains approximately constant for $D \gtrsim 2.3$. Taking into account that in this range the volume occupied by the inner vortex does not change anymore [Figs. 9(g) and 9(h)], we

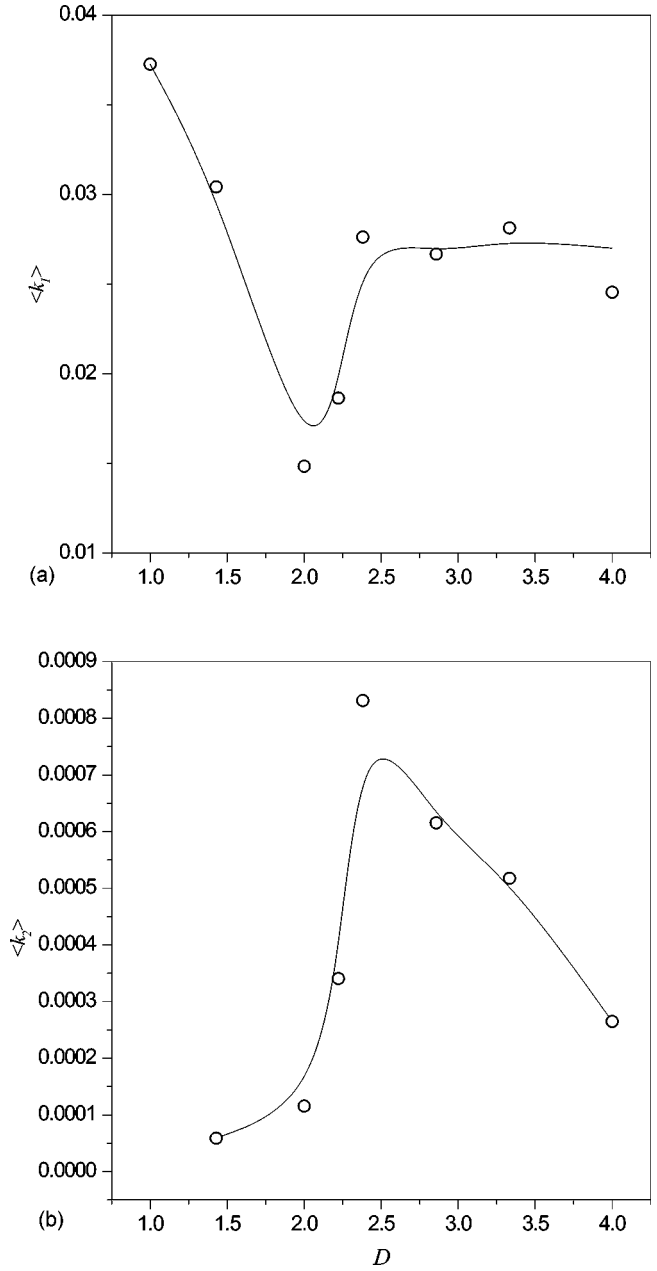

FIG. 12. Kinetic energy density of the inner, counterclockwise rotating vortex (a) and the outerclockwise rotating region (b), as functions of D for $\Gamma=1$, $\mathrm{Re}=900$. The symbols indicate numerical simulation data, while the solid line represents a curve fit. The inner vortex remains unaffected by D for $D>2.3$, while the growth of the outer vortex involves only very low velocity regions.

conclude that the motion of the inner vortex is maintained at a constant kinetic energy density by the rotating disk.

A relatively small fraction of the overall energy is transferred to the outer vortex, whose volume increases as D grows. At the same time, the velocity field in the outer vortex becomes nearly independent of D as $D \gtrsim 2.3$. All of the growth of the outer vortex involves regions of very small velocities. Consequently, the kinetic energy density of the outer vortex decreases with increasing D, as shown in Fig. 12(b).

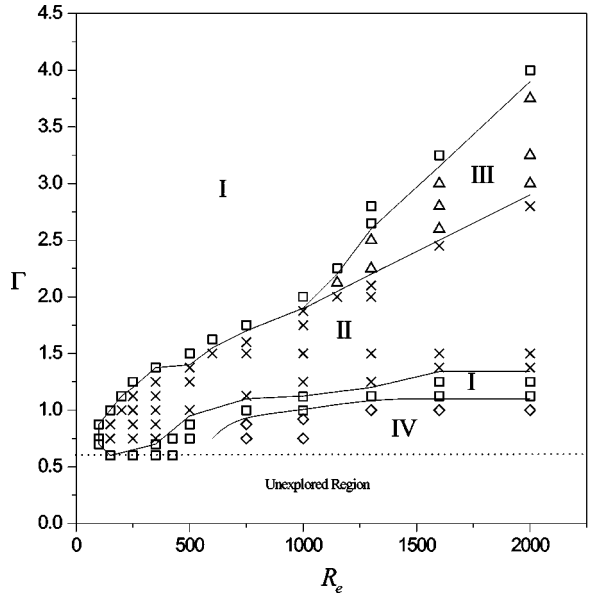

FIG. 13. Onset of vortex breakdown bubbles in the parameter plane (Re, Γ, $D=2.5$). Four regions can be distinguished, viz., region I (□, no bubble); II (×, one surface bubble away from the axis); III (△, one internal bubble); and IV (◇, corner bubble). No simulations were conducted for $\Gamma<0.6$.

C. Onset of vortex breakdown

In order explore a wider parameter range, we now discuss results for a fixed value $D=2.5$ of the horizontal aspect ratio, and for Γ and Re varying in the ranges $0.3<\Gamma<4$ and $50<\mathrm{Re}<2000$. For certain combinations of these parameters a third type of bubble, termed "internal bubble," forms whose two stagnation points are both located on the axis of rotation. This type of vortex breakdown structure was also observed in Sec. IV for $D=1$ and $\mathrm{Re}=425$, cf. Fig. 4(b). In this context it should be pointed out that our detection method for vortex breakdown structures is based on a purely visual inspection of the streamline pattern. A bubble is said to be present when a nonzero area of clockwise circulation is enclosed by a $\psi=0$ contour. We typically observe that near the onset a slight increase in Re, at fixed value of Γ, produces a rapid growth of the bubble, in agreement with the findings of Ref. 30.

Overall, the (Re, Γ, $D=2.5$) plane shows four distinct regions, cf. Fig. 13: region I without bubbles, region II with a surface bubble away from the axis, region III with an internal bubble, and region IV with a corner bubble. In comparison to the phase diagram obtained by Spohn *et al.* for (Re, Γ, $D=1$), we note a few differences. For a fixed Γ value the onset of vortex breakdown for $D=2.5$ occurs at smaller Reynolds number than in the $D=1$ experiments by Spohn. For $\Gamma \lesssim 2.65$, the diagram by Spohn *et al.* shows a narrow band of Reynolds numbers with internal bubbles, while for $D=2.5$ internal bubbles appear only in a narrow band for $\Gamma>2.25$.

This behavior can be explained in light of the arguments provided in Sec. IV: for $D=2.5$ the lateral wall is located well beyond the region where the separated boundary layer attaches to the free surface, so that the angular momentum created by the spinning disk reaches the free surface without

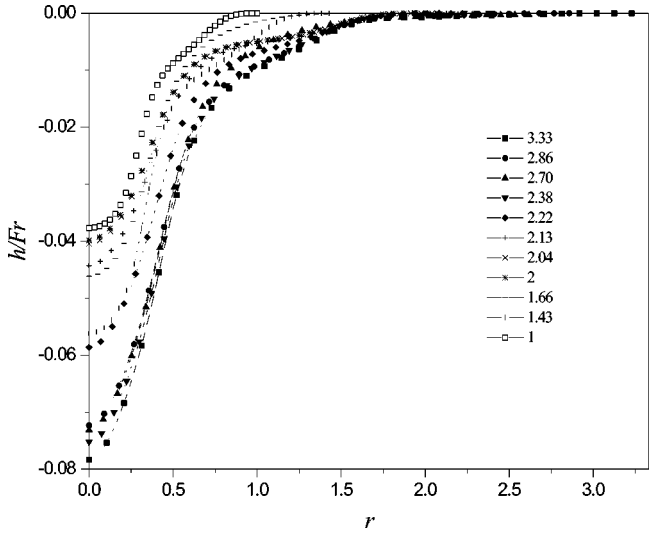

FIG. 14. Surface deflection for $\Gamma=1$, Re=900, and various ratios D. The largest surface deflections are observed for $D>2.38$, when a strong outer vortex exists.

significant losses. However, it does so at a much larger radius than for $D=1$. Since angular momentum is approximately conserved along the free surface, the inward radial fluid motion thus comes to a halt at a radius on the free surface which is larger for $D=2.5$ than for $D=1$, where the lateral wall imposes causes dissipative losses. Consequently, $D>1$ is seen to promote the appearance of a bubble attached to the free surface, especially for small values of Γ. On the other hand, for large Γ the dissipation of angular momentum by viscosity can no longer be neglected. Hence the fluid at the free surface can move to small radii before it is deflected downward, so that the occurrence of internal bubbles is favored.

V. SURFACE DEFLECTION

Based on the above steady state, axisymmetric results, it is possible to determine the leading order free surface deflection $h(r)$ that the flow would develop if it was allowed to deform under the influence of gravity, pressure, and viscous forces. From the balance of the normal stresses we obtain, in dimensionless form

$$\frac{1}{\mathrm{Fr}}h - p + \frac{2}{\mathrm{Re}}\frac{\partial w}{\partial z} = 0, \tag{17}$$

where the Froude number Fr is defined as

$$\mathrm{Fr} = \frac{\Omega^2 R_d}{g}. \tag{18}$$

Figure 14 depicts the surface deformation profiles for some of the flow fields shown in Fig. 9, with $\Gamma=1$, Re =900, and several values of D. We find that the surface shapes for $D>2.38$, when the strong outer vortex exists, are clearly distinct from the rest of the curves.

VI. CONCLUDING REMARKS

Qualitative changes of the fluid motion in a cylindrical container with one rotating end wall are observed when the lateral wall is moved radially outward, so that the outer section of the end wall is at rest. The present study focuses on this configuration for the case of a free surface, as a natural extension of the earlier work by Spohn *et al.*[15,16]

As the main observation, we find that the flow above the stationary part of the end wall is dominated by the mechanism first described by Bödewadt:[26] The rotating fluid motion above the stationary end wall generates a pressure field that increases with the radius. Within the viscous boundary layer on the stationary end wall, this pressure distribution is not balanced by a corresponding centrifugal force, so that a radially inward flow results. As this flow approaches the edge of the rotating disk, it encounters the radially outward flow set up by the spinning disk, so that fluid separation occurs. Hence a flow configuration results that is dominated by a counterclockwise vortex above the spinning disk, and a clockwise rotating vortex above the stationary part of the end wall.

As the ratio of container radius to disk radius increases above a value of about 2.3, the influence of the lateral container wall on the features of the central flow in the neighborhood of the spinning disk becomes insignificant. By means of a simplified model problem, it is demonstrated that this rapid loss of influence is due to the exponential decay of the azimuthal surface velocity beyond the edge of the disk. This exponential decay is confirmed by the numerical data, and it reflects the fact that as the lateral wall moves outward, the stationary part of the end wall becomes the main sink for the azimuthal momentum of the fluid.

A series of simulations for various aspect ratios and Reynolds numbers demonstrates that the outward shift of the container wall modifies the vortex breakdown configurations as well, and the physical reasons for these changes are discussed.

Several attractive avenues exist for future extensions of the current investigation. First of all, accompanying experiments by one of the authors (Ref. 29) show that for D =3.33 the main flow features concide with those described above, and that the flow can become time dependent for Re$>$300. It would be interesting to unravel the instability mechanism behind this transition, and to investigate its influence on such flow properties as the global mixing efficiency. In this context, it might also be attractive to evaluate strategies for the control of the flow, for example, by varying the rotation rate of the spinning disk in a time-dependent fashion, and/or by rotating the cylindrical container wall, which would affect the relative strengths of the two main vortical structures. Finally, it will be of interest to study three-dimensional flow features as well.

ACKNOWLEDGMENTS

This work was initiated while both authors were visiting the Laboratoire de Physique et Mécanique des Milieux Hétérogènes at ESPCI, Paris, France. The hospitality of this group is warmly acknowledged.

[1]T. von Karman, "Laminare und turbulente Reibung," Z. Angew. Math. Mech. **1**, 233 (1921).
[2]H. U. Vogel, "Experimentelle Ergebnisse über die laminare Strömung in einem zylindrischen Gehäuse mit darin rotierender Scheibe," MPI Bericht 6, 1968.
[3]H. U. Vogel, "Rückströmungsblasen in Drallströmungen," Festschrift 50 Jahre Max-Planck-Institut für Strömungsforschung, 1975.
[4]M. P. Escudier, "Observations of the flow produced in a cylindrical container by a rotating endwall," Exp. Fluids **2**, 189 (1984).
[5]M. R. Ruith, P. Chen, E. Meiburg, and T. Maxworthy, "Three-dimensional vortex breakdown in swirling jets and wakes," J. Fluid Mech. **486**, 331 (2003).
[6]M. A. Herrada, M. Prez-Saborid, and A. Barrero, "Vortex breakdown in pipes: Compressibility and 3D effects," Bull. Am. Phys. Soc. **48**, 114 (2003).
[7]H. J. Lugt and H. J. Haussling, "Axisymmetric vortex breakdown in rotating fluid with a container," J. Appl. Mech. **49**, 921 (1982).
[8]H. J. Lugt and M. Abboud, "Axisymmetric vortex breakdown with and without temperature effects in a container with a rotating lid," J. Fluid Mech. **179**, 179 (1987).
[9]J. M. Lopez, "Axisymmetric vortex breakdown. Part 1. Confined swirling flow," J. Fluid Mech. **221**, 533 (1990).
[10]G. L. Brown and J. M. Lopez, "Axisymmetric vortex breakdown. Part 2. Physical mechanisms," J. Fluid Mech. **221**, 553 (1990).
[11]M. A. Herrada and V. Shtern, "Vortex breakdown control by adding near-axis swirl and temperature gradients," Phys. Rev. E **68**, 041202 (2003).
[12]T. Maxworthy, "Laboratory models of rapidly swirling flows with application to atmospheric vortices," Astronaut. Acta **17**, 363 (1972).
[13]T. Maxworthy, "A vorticity source for large scale dust devils and other comments on naturally occurring columnar vortices," J. Atmos. Sci. **30**, 1717 (1973).
[14]T. Maxworthy, "The laboratory modeling of atmospheric vortices: A critical review," in *Proceedings of the IUTAM Conference on Intense Atmospheric Vortices*, *Reading*, *England* (Springer, New York, 1981).
[15]A. Spohn, M. Mory, and E. J. Hopfinger, "Observations of vortex breakdown in an open cylindrical container with a rotating bottom," Exp. Fluids **14**, 70 (1993).
[16]A. Spohn, M. Mory, and E. J. Hopfinger, "Experiments on vortex breakdown in a confined flow generated by a rotating disk," J. Fluid Mech. **370**, 73 (1998).
[17]O. Daube, "Numerical simulation of axisymmetric vortex breakdown in a closed cylinder," Lect. Appl. Math. **28**, 131 (1991).
[18]D. T. Valentine and C. C. Jahnke, "Flows induced in a cylinder with both end walls rotating," Phys. Fluids **6**, 2702 (1994).
[19]J. M. Lopez, "Unsteady swirling flow in an enclosed cyclinder with reflectional symmetry," Phys. Fluids **7**, 2700 (1995).
[20]M. Brons, L. K. Voight, and J. N. Sorensen, "Topology of vortex breakdown bubbles in a cylinder with a rotating bottom and a free surface," J. Fluid Mech. **428**, 133 (2001).
[21]J. M. Lopez, F. Marques, A. H. Hirsa, and R. Miraghaie, "Symmetry breaking in free-surface cylinder flows," J. Fluid Mech. **502**, 99 (2004).
[22]J. M. Lopez and F. Marques, "Mode competition between rotating waves in a swirling flow with reflection symmetry," J. Fluid Mech. **507**, 265 (2004).
[23]D. L. Young, H. J. Sheen, and T. Y. Hwu, "Period-doubling route to chaos for a swirling flow in an open cyclindrical container with a rotating disk," Exp. Fluids **18**, 389 (1995).
[24]A. H. Hirsa, J. M. Lopez, and R. Miraghaie, "Symmetry breaking to a rotating wave in a lid-driven cylinder with a free surface: Experimental observation," Phys. Fluids **14**, L29 (2002).
[25]R. Miraghaie, J. M. Lopez, and A. H. Hirsa, "Flow induced patterning at the air/water interface," Phys. Fluids **15**, L45 (2003).
[26]U. T. Bödewadt, "Die Drehströmung über festem Grunde," Z. Angew. Math. Mech. **20**, 241 (1940).
[27]C. A. J. Fletcher, *Computational Techniques for Fluid Dynamics* (Springer, Berlin, 1988).
[28]W. H. Press, B. P. Flannery, S. A. Teukolsky, and W. T. Vetterling, *Numerical Recipes* (Cambridge University Press, Cambridge, 1989).
[29]M. Piva, "Estructuras de recirculación en un contenedor cilindrico," Ph.D. thesis, Universidad de Buenos Aires, 2000.
[30]T. Mulin, J. S. Tavener, K. A. Cliffe, "On the creation of stagnation points in a rotating flow," Proc. ASME OED/Intnl. Cong. Sym. **1**, 3 (1997).